Experimental study of bubble sweep-down in wave and current circulating tank: Part I—Experimental set-up and observed phenomena

Sylvain Delacroix [a], Grégory Germain [a,*], Benoît Gaurier [a], Jean-Yves Billard [b]

[a] IFREMER, Marine Structures Laboratory, 150 Quai Gambetta, 62321 Boulogne-sur-Mer, France
[b] IRENAV, Ecole Navale, 29240 Brest, France

A B S T R A C T

Bubble sweep-down is a significant issue for the oceanographic vessels, which affect the acoustic surveys. Experimental trials, carried out in the Ifremer wave and current circulating tank on a 1/30 model of the *Pourquoi pas?*, are presented. The results demonstrate that this kind of experimental facility is well suited to study the phenomenon of bubble sweep-down encountered around the bow of a ship under specific conditions. From these results, two kinds of bubble clouds formation have been observed and analysed: bubble clouds generated by vortex shedding and breaking waves. The vortex shedding bubble clouds appear randomly in all the configurations tested, even without waves or motions. This phenomenon is due to the interaction between the turbulent flow and the specific bow shape of the *Pourquoi pas?*. On the other hand, the breaking wave clouds appear in the presence of relative motions between the free surface and the bow ship and more significantly under wave sollicitations. A complementary paper presents a parametric study carried out to quantify the influence of the test conditions.

Keywords:
Bubble sweep-down
Experimental trials
Ship motions
Bow waves

1. Introduction

The ocean is an opaque environment where the light only propagates over several meters. The observation of fisheries or seabed topography are consequently complex and require the use of acoustic waves able to propagate over several kilometres and carry back information after reflection on an obstacle. Specific acoustic equipments, single or multi-beam echosounders, are used on oceanographic vessels for many varieties of research. These echosounders are calibrated to work precisely in seawater, independently of the water temperature and density. Ship motions can also be compensated. However the acoustic waves can be strongly disrupted (reflected or absorbed) if air bubbles are present in the sea layer under the hull. This phenomenon has affected the acoustic surveys for many years (Dalen and Løvik, 1981; New, 1992) and is still a significant issue (Shabangu et al., 2014).

The bubble distribution in the upper ocean is caused by two main sources. Natural aeration is mostly due to the entrapment of air by breaking waves and rain impacting on the ocean surface. Several works have been dedicated to this topic, motivated by gas exchanges between the ocean and the atmosphere. Chanson and Cummings (1994) described a theoretical method to predict the size and the depth of entrained bubbles. Deane and Stokes (1999, 2002) developed an optical system able to record bubbles of radii >200 μm. Trevorrow (2003) used a high frequency sonar for the measurements of near-surface bubble plumes in the upper ocean layer. All these studies demonstrated that micro-bubbles are dispersed by turbulence to depths of several meters (up to 25 m according to Trevorrow) in bad weather conditions. On the other hand, the ship bow wave generates a significant aeration, and the flow around the hull may carry self-generated bubbles under sonar locations. This phenomenon of bubble sweep-down, favoured by ship motions, must be prevented as much as possible in order to ensure a good productivity for a ship dedicated to acoustic survey.

Rolland and Clark (2010) have compared several solutions adopted to avoid bubble sweep-down. Gondolas, fairings and bubble fences can effectively reduce bubble sweep-down but generally significantly increase the ship resistance. During the design of the future Research Vessels *Discovery* and *Sonne*, particular attention was given to the bubble sweep-down issue (Cooper, 2012; Von Bröckel, 2014). From past experiences, general conclusions are given as the benefit of a deep draft, or to avoid bulbous bow. However, considering all these elements does not guarantee the reduction of bubble sweep-down. Indeed the Research Vessel *Pourquoi pas?* of Ifremer fleet, although equipped

with a gondola, has encountered significant bubble sweep-down interferences since the first sea trials in 2005 (Delacroix et al., 2016).

The tools allowing the study of this phenomenon are limited. Numerical simulations of this kind of diphasic problem are still difficult to achieve because of the scale difference between bubbles production, governed by surface tension, and the flow all around the hull. Moraga et al. (2008) developed a physically-based model that locates the region of high void fraction. The model uses the bubble size distribution measured by Deane and Stokes (2002) to simulate the bubbly flow around the hull of the research vessel *Athena* with the prediction of air bubble locations. Ma et al. (2011) describe a subgrid model coupled with a two-fluid Reynolds Average Navier Stokes (RANS) bubbly flow model, and obtain the first quantitative numerical prediction of void fraction distributions around a full-scale surface ship. Lately Carricaetal (2012) and Castroetal (2014) improved the air entrainment model, taking into account turbulent and cavity free surface bubble entrainment. All these investigations have been performed in calm seas, without ship movements. To this point therefore, numerical studies used for bubble sweep-down consideration during ship designs are only based on the analysis of streamlines without waves and motions. The effect of different sea state is investigated by model test in towing tank. However, the generation of bubbles is usually low or non-existent around the model because of scale effects, and the evolution of the bubbles is simulated by dye injection at the bow vicinity. Conclusions of the these kind of tests are not always verified at sea (*Pourquoi pas?* experience and Von Bröckel, 2014). Specific experiments have already been developed to study the bow wave geometry (Noblesse et al., 2008, 2013; Delhommeau et al., 2009) and the resulting air entrainment (Waniewski et al.; Shakeri et al., 2009; Tavakolinejad, 2010), but these studies focused on steady bow wave in calm seas for thin and fast ships. The influence of sea states and motions have not been considered.

We propose here an original experimental method under which the phenomenon can be studied. This method is based on the simulation, in a wave and current circulating tank, of sea conditions encountered by the French oceanographic vessel *Pourquoi pas?* during which bubble sweep-down was observed. We present in the first part of this paper the details of the experimental set-up and the two kinds of aeration phenomenon encountered by this way, while the analysis of the bubble clouds is described in the second part of the paper.

2. Experimental set-up

This section aims at giving a thorough description of the experimental set-up and measurement facilities used for this study. The *Pourquoi pas?* is operated by Ifremer and the French Ministry of Defence, primarily for hydrography, submarine cartography and seabed characterization. Its main characteristics are a length between perpendiculars $L_{pp} = 94$ m, a beam $B = 20$ m and a draft $T = 5.45$ m in operation. This vessel has been chosen for the considerable database of sea campaigns which is easily accessible, and the significant effect of bubble sweep-down on the acoustic equipments.

2.1. Wave and current circulating tank facilities

This experimental technique has been developed in the wave and current circulating tank of Ifremer (in Boulogne-sur-mer, France). In such facility, the model is fixed and the ship velocity is simulated by the current. The tank working section is 18 m long by 4 m wide and 2 m deep (see Fig. 1). Regarding scale effects, the model must be large enough to be able to observe bubble sweep-down. Therefore, the maximum scale have been chosen, taking into account the tank characteristics. A 1/30 model of the *Pourquoi pas?* allows to generate trials conditions with relatively low blockage and reflection effects in the bow vicinity. That scale corresponds to a ship model of 3.13 m length between perpendiculars (Lpp), 0.67 m beam and 0.18 m draft (see Fig. 2).

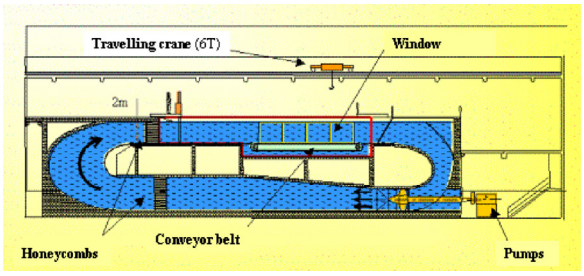

Fig. 1. Schematic view of the wave and current circulating tank.

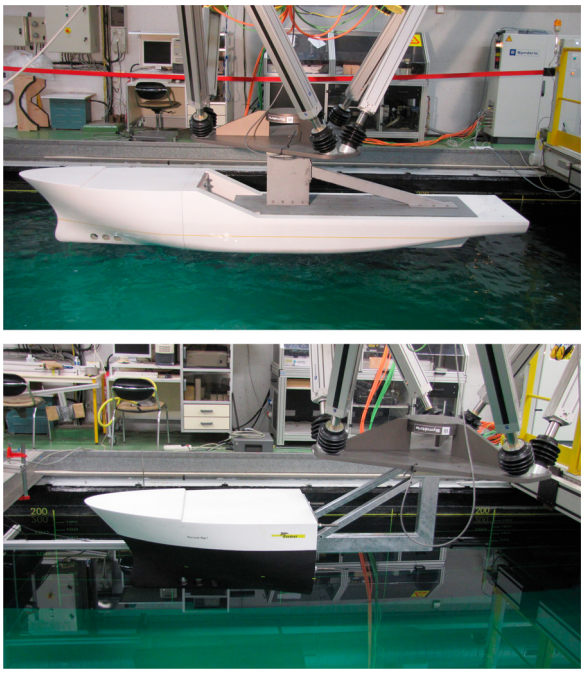

Fig. 2. 1/30 model of the *Pourquoi pas?* fixed under the hexapod. Top: full model. Bottom: bow model only with the same relative position to the hexapod center of reference than for the full model.

The circulating tank is equipped with a wave generator composed of 8 independent displacement paddles each 0.5 m wide and 0.5 m deep, which can be easily moved between an upstream or a downstream surface position in order to create waves propagating with or against the current. This wave generator enables the production of regular and irregular waves with a frequency range between $f = 0.5$–2 Hz and a maximum amplitude of $A = 280$ mm with a current up to 0.8 m/s. Measurements revealed that the resulting reflection coefficient is lower than 12% for all the usual wave frequencies and amplitudes. More details about the flume tank can be found in Gaurier et al. (2013) and Bouhoubeiny et al. (2014). The free surface elevation is measured by the mean of a wave gauge system with the wave probe situated 1 m upstream from the model bow.

When the wave generator is located upstream, there is a high turbulent intensity (TI) in the incoming flow. $TI = 15\%$ in this configuration, close to sea turbulence, while without the wave generator, the turbulent intensity is $TI = 3\%$, with:

$$TI = \sqrt{\frac{1}{3}\frac{u'^2 + v'^2 + w'^2}{\overline{u}^2 + \overline{v}^2 + \overline{w}^2}} \quad (1)$$

Thanks to the Reynolds decomposition, $U = \overline{u} + u'$ where $\overline{u}$ is the mean value and u' the fluctuating part of the current velocity U. The corresponding data have been measured with a 2D Laser Doppler Velocimetry system in two steps to acquire the three velocity components.

The major difference between this configuration and classic towing tank tests, during which models are free to heave and pitch, is that the ship motions are here forced by a motion generator system (hexapod).

This system allows to generate any motions in the 6 degrees of freedom. It is not necessary then to have a balanced ship model in terms of displacement, inertia and center of gravity, which greatly facilitate the design and construction of the scale model. The use of the motion generator also enables to study independently the effect of waves and motions on bubbles production. Above all, in this configuration it is possible to work with the front part only (1/3 of the model). This possibility is very interesting in a relatively small circulating tank where perturbations coming from the model stern motions are indeed avoided.

The two different configurations are shown in Fig. 2. Measurements of the ship resistance were performed on the full model configuration. It has been shown that the flow in the circulating tank is representative of the real scale flow as in the classic towing tanks (Delacroix, 2015). After verification that the tests with the front part only have no influence on the flow in the bow region, all the study of bubble sweep-down have been undertaken in this configuration, in order to suppress the waves generated by the relatively flat end part of the *Pourquoi pas?* model.

The ship model motions are measured by the mean of the hexapod real time measurement system, with a precision of less than 0.1 mm and 0.01°.

The computer program FREDYN has been used for the calculation of the ship motions taking into account the experimental conditions. In this program, a nonlinear strip theory approach is used to compute the hydrodynamic forces acting on the hull (De Kat and Paulling, 2001). In the time domain simulation the ship motion components are determined from a set of six coupled differential equations of motion. Integration of the calculated accelerations provides the velocities and a second integration leads to the ship position at each time step.

The model is defined by the geometry, the ship resistance, and the characteristics of the propellers and rudders (see Fig. 3). Then the conditions of calculation are defined (rotation of the propeller, waves spectrum and direction). The validation of this numerical model is based on the results of the *Pourquoi pas?* seakeeping tests from MARIN obtained on a 1/16.7 scale model (Technical Report, 2003). The configurations tested with irregular seas are shown in Table 1, where H_s is the significant wave height and T_p the peak period of the wave spectrum.

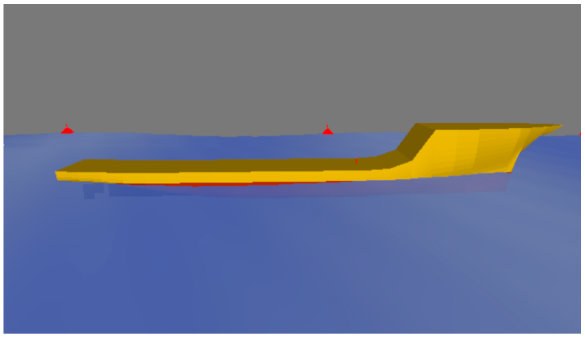

Fig. 3. FREDYN numerical model of the *Pourquoi pas?*.

Table 1
Configurations tested for the numerical model validation.

Configuration	1	2	3	4	5
V (knots)	5	10	5	9	5
H_s (m)	3.25	3.25	5	5	6.25
T_p (s)	9.7	9.7	12.4	12.4	12.4

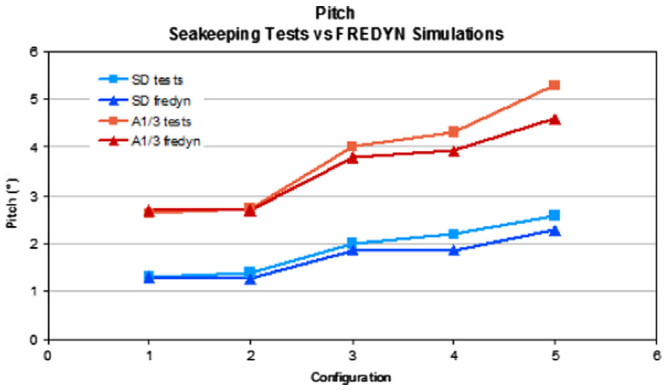

Fig. 4. Comparison of Fredyn and seakeeping test results for several sea state conditions.

The results of FREDYN calculations for these configurations are shown in Fig. 4. In the graphics we can see the statistical analysis of pitch obtained for each configuration in terms of standard deviation and significant amplitude (mean of the third highest amplitudes). The pitch is slightly lower for the numerical model for the highest wave amplitude, but the trends are good and the results are very similar for configuration 1 and 2 (respectively 0% and 8.7% of error for the standard deviation, and 2.3% and 1.5% for the significant amplitude). These configurations are close to the trial conditions, described in Section 3, and validate the numerical model.

2.2. Instrumentation

The first objective of these experiments is to observe and characterize the phenomenon of bubbles generation around the bow. To this aim two synchronized video systems were used: a Tomography system used to obtain very good quality of underwater images, and two high performance digital CMOS cameras for the visualization of the free surface in the bow vicinity. Both systems acquired images at a 15 Hz frequency.

The tomography system is based on a two-cavities Gemini Nd–Yag laser (2×120 mJ/pulse at 15 Hz), using an excitation wavelength of 532 nm. The laser sheet is emitted in the water, by the use of a laser guiding arm in order to generate a light sheet on the vertical plane along the main axis of the ship model (see Fig. 5), far enough of the bow in order to prevent flow perturbations in the measurement area. The camera (Hi-sense CCD camera) records single-frame images in this configuration with a 1600×1200 pixels^2 resolution. The distance between the camera—located perpendicularly—and the laser sheet is 2.2 m so that the image size obtained is 36×27 cm^2 with a magnification factor of 0.225 mm/pixel.

The experimental set-up is summarized in Fig. 6 illustrations.

3. Test configurations

Before presenting the test parameters and the selected tests configurations, it is necessary to discuss about similarity issues

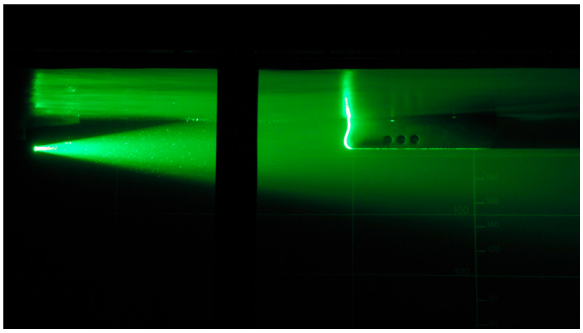

Fig. 5. Laser sheet in the ship model axis for the acquisition system in the bow vicinity of the *Pourquoi pas?*

and scale effects. Indeed, these effects are potentially prohibitive for this kind of study, on a 1/30 scale model of an oceanographic vessel in a wave and circulating tank.

3.1. Similarity issues

The aim of this work is to have a better understanding of the ship behaviour regarding the generation and propagation of air bubbles. The most important elements involved in these phenomena are waves and ship motions. Therefore, the experimental study requires to observe the Froude similitude ($Fr = V/\sqrt{gL_{pp}}$ and in this case Fr=0.203). Hence, a good representation of the free surface influence is ensured. In this case, the first consequence is to work at a different Reynolds number between tests and real scale. Based on the ship speed V, and the ship length between perpendiculars L_{pp}, the Reynolds number defined as: $Re = VL_{pp}/\nu$ is respectively $Re_{model} = 2.1 \times 10^6$ in the experiments and $Re_{ship} = 3.4 \times 10^8$ at full scale. Then the flow would significantly be less turbulent around the model. On the other hand, there is a high turbulent intensity in the tank, due to the presence of the wave generator upstream as detailed in Section 2.1. The lower Reynolds number at model scale may affect the boundary layer very close to the hull, but not the propagation of bubble clouds that are generated outside this thin layer (of the order of few mm).

Similarity issues are also important for the bubbles behaviour. First of all, the Froude similarity means smaller wave amplitudes, a lower flow velocity and consequently lower energy in the flow around the model. The quantity of air entrapped under the free surface is consequently reduced. Moreover, the size of the bubbles in the flow is determined by a balance between shear stresses, inertia and surface tensions. This issue is associated to the Weber number, defined here with the ship incoming wave amplitude: $We = \rho AV^2/\sigma$, which cannot be conserved during the tests: $We_{model} = 2.5 \times 10^3$ in the experiments and $We_{ship} = 2.3 \times 10^5$ at full scale. Shear stresses are insufficient to generate microscopic bubbles as can be observed at sea. Several millimetres is the typical size for bubbles in tank, which will have a greater rise velocity. Moreover the salinity of the water directly affects bubble size distribution, limiting coalescence events as explained by Cartmill and Su (1993) and Kracht and Finch (2009), increasing the quantity of small bubbles at sea.

All these elements make difficult the observation of bubble sweep-down in classic towing tank as well as direct extrapolation to real scale. However, the original experimental method described below enables a good visualisation and a better apprehension of the phenomenon.

The three significant dimensionless numbers are summarised in Table 2 for both model at 1/30 scale and ship at real scale cases.

3.2. Test parameters

Shortly after the first cruises of the *Pourquoi pas?*, specific tests at sea (*Essbulles* cruise, 2005) were performed to characterize disturbances on sonar acquisition. These tests showed that such disturbances were due to bubble clouds, confirmed by video measurements from the gondola, and correlated with the pitch in head sea navigation. Bubble sweep-down was observed at sea for the conditions (velocity, wavelength, significant wave height and wave period) given in Table 3.

The first step for the experimental study of bubble sweep-down in circulating tank is to reproduce these conditions as close as possible, with current, waves and ship motions. In this case, ship motions are imposed by the use of an hexapod, synchronized

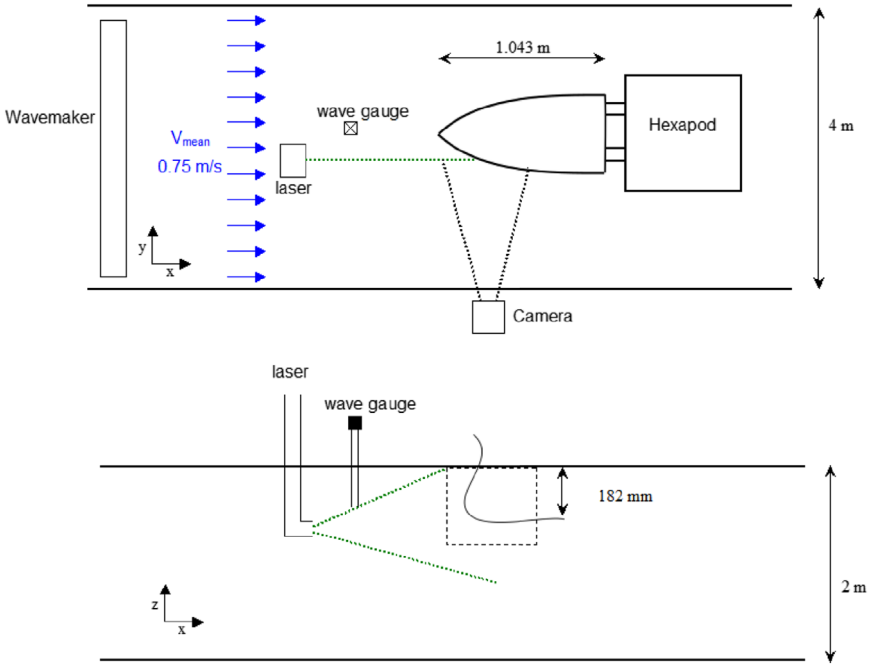

Fig. 6. Drawing of the experimental set-up, top and side view showing the light sheet generation system location.

Table 2
Main parameters and dimensionless numbers for the tests and at real scale.

Case	L_{pp} (m)	V (m/s)	Fr	Re	We
Ship	94	4.12	0.203	3.4×10^8	2.5×10^3
Model	3.13	0.75	0.203	2.1×10^6	2.3×10^5

Table 3
Sailing conditions during the *Essbulles* cruise, 2005.

V (knots)	λ (m)	H_s (m)	T_p (s)
8	109	2.8	8.4

with the wave generator. To this end, it is necessary to work with regular waves. In these conditions the uncertainty of the waves and resulting motions is suppressed, which prevents extreme events. The characteristics of the regular waves will be calculated to conserve the energy density of the conditions encountered at sea.

The energy density of irregular waves is given by the following expression:

$$E = \rho g m_0 [J/m^2], \quad \text{with } H_s = 4\sqrt{m_0} \tag{2}$$

where m_0 is the zero order moment of the wave energy spectra.

For sinusoidal waves:

$$E = \frac{1}{2}\rho g A^2, \quad \text{where } A \text{ is the amplitude } (A = H/2). \tag{3}$$

To observe energy density conservation, one must write:

$$m_0 = \frac{1}{2}A^2 \tag{4}$$

$$\text{so } A = \frac{\sqrt{2}H_s}{4} \quad \text{and} \quad H = \frac{\sqrt{2}H_s}{2} \tag{5}$$

For $H_s = 2,8$ m the sinusoidal waves with the same energy density will have a wave height $H = 2,0$ m. The period T will be taken equal to T_p.

The input characteristics of the regular waves for the wave generator are the amplitude and the frequency. The current and the wave amplitude for the trials are directly obtained by the Froude scaling. At the model scale the ship speed is $U = V/\sqrt{30} = 0.75$ m/s. The wave amplitude is $A_m = A_r/30 = 33$ mm. For the calculation of the frequency it must be taken into account that the model is fixed and the encounter frequency is higher than that of the wave. The encounter frequency is given by

$$f_e = f - \frac{V}{\lambda}\cos(\theta) \tag{6}$$

with θ=0° for following sea and 180° for head sea. So in our configuration:

$$f_e = f + \frac{V}{\lambda} \tag{7}$$

We finally obtain $f_e = 0,85$ Hz, and the final trial conditions are summarized in Table 4. The generation of waves in the tank is

Table 4
Trial main parameters.

U (m/s)	A (mm)	f_e (Hz)
0.75	33	0.85

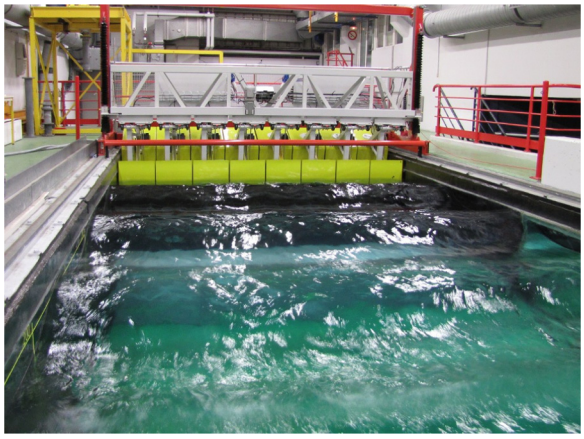

Fig. 7. Illustration of regular wave generation in the tank with a current of 0.75 m/s.

illustrated in Fig. 7.

After the numerical model validation and the determination of trial conditions, ship motions are calculated with the use of the Fredyn model. The calculation inputs correspond to regular waves of 2.0 m height and 8.4 s period and a ship velocity of 8 knots. The full scale results are shown in Fig. 8. Surge movements, not represented on the graphic, are insignificant (<0.1 m at full scale) and will not be taken into account during this study. In this head sea configuration, the only significant movements are the heave and the pitch. It must be emphasized here that wave and heave are in-phase.

These results must be converted to model scale by Froude scaling ($\times 1/\sqrt{30}$ for the time, $\times$ 1/30 for the heave and $\times$ 1 for the pitch). It is finally obtained 2° pitch and 20 mm heave model motion amplitudes.

3.3. *Wave and motion synchronism*

A key point of the methodology is the synchronisation of the waves and motions. For that purpose a start-up procedure has been developed and is summarized in Fig. 9. The user starts the wave generator sequence, which sends a trigger signal that starts the hexapod sequence. In this sequence a pause time must be inserted for the wave to reach the model. The phase shift between wave and motion is adjusted by this pause time. The hexapod sequence also sends a trigger signal that starts simultaneously all measurement systems (laser, cameras, motions acquisition system, waves gauges).

The synchronism is verified *a posteriori* with the motions and wave recording as can be seen on Fig. 10. The free surface elevation

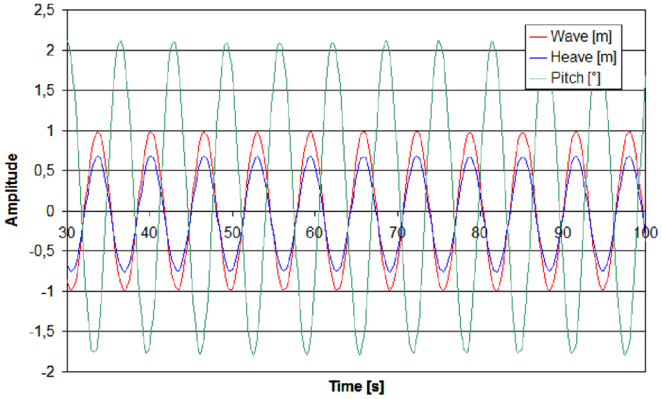

Fig. 8. FREDYN results for the trial conditions at real scale.

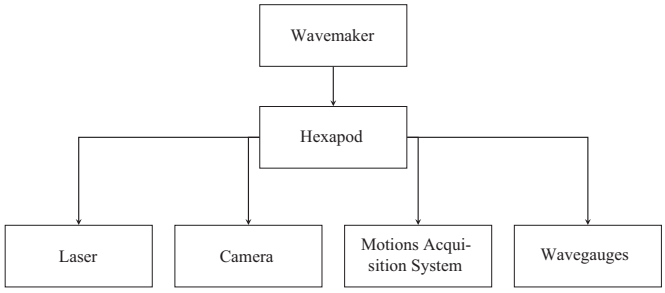

Fig. 9. Synchronism diagram of the experimental set-up between the wavemaker, the hexapod and the dedicated instrumentation.

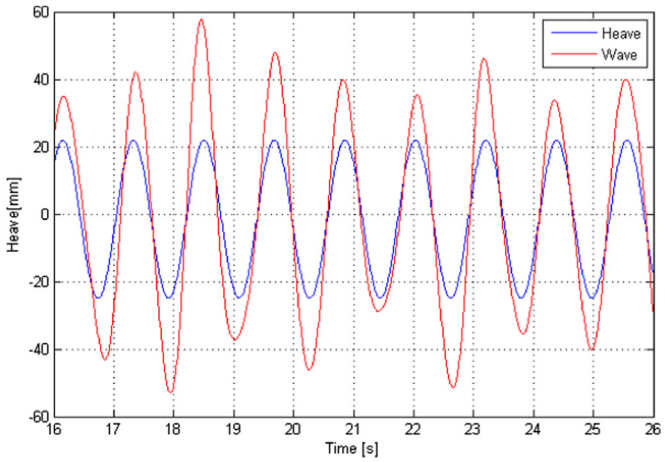

Fig. 10. Example of waves and heave synchronisation from the experimental measurements with a current of 0.75 m/s.

at the model center of gravity is obtained from measurement 1 m upstream the bow. Previous tests with 2 wave gauges were undertaken to calculate the wave celerity.

Motions generated by the hexapod as well as wave frequency are extremely precise while wave amplitude fluctuations are important due to the interaction between the current and the wave generator. The standard deviation of the wave amplitude is 13 mm and less than 0.1 mm for the measured heave amplitude. The mean phase shift is calculated on the whole sequence, and only the sequences with less than 10° of mean phase shift for which there is no influence on bubble generation occurrence are conserved for the analysis. Because the wave amplitudes fluctuate but motions do not, the imposed motions calculated with Fredyn are not reproducing the proper motion for a free model on every period. It will result in more violent forces in some periods, inducing more bubble entrainment, or the opposite at other periods. For such reasons many analysis of bubble clouds generation were performed on single periods separately, selected by the wave amplitude. A wave by wave analysis is preferable than a statistical one.

3.4. Test configurations

The final objective of this work is to understand bubbles generation and propagation around the hull, to be able to offer solutions to minimize the phenomenon. Several configurations have been tested to apprehend the influence of each parameter.

- In the first configuration (case 1), the model is fixed and only submitted to the circulating tank current (U=0.75 m/s).
- In the second configuration (case 2), the model is fixed and submitted to current and regular waves (33 mm amplitude and 0.85 Hz frequency).
- In the third configuration (case 3), motions are forced by the hexapod (2° pitch and 20 mm heave at 0.85 Hz), and the model is submitted to current.
- In the fourth configuration (case 4), the model is submitted to current, as well as synchronized waves and motions.

4. Bubble sweep-down phenomenon

In this section, we first describe the phenomena observed through the experimental method developed above, from observations of the free surface behaviour at the bow, and of the bubble clouds in the water column. Secondly, bubble clouds occurrence is discussed for the four configurations.

4.1. Visualization of bubble generation

Through the experimental configurations described in Section 3, two different air entrainment mechanisms have been detected. In the following these two kinds of bubble cloud will be referred respectively as vortex shedding cloud and breaking wave cloud. These phenomena are completely independent and easy to distinguish, even if for very few cases both air entrainment mechanisms can occur at the same time. For these particular events, we are also able to distinguish each of them.

The first kind of air entrainment is encountered in all configurations, even without waves and motions. In this case, the incoming turbulent flow generates a distortion of the free surface in contact with the bow. A small air cavity is developed until the air entrapment by vortex shedding. The initiation of this phenomenon may be held for several tenths of seconds. This phenomenon appears randomly throughout the test sequence, but with a stable frequency of occurrence. A schematic description of the vortex entrainment mechanism is presented in Fig. 11.

The formation of the cavity occurs when the flow shows a high velocity gradient at the bow contact, with plunging and ascending speeds relatively close. When the velocity gradient becomes too large, the cavity widens and becomes unstable. Then the appearance of a vortex may be observed (whose main axis is transverse to the measurement plane), causing air entrainment and the generation of the corresponding bubbles cloud.

The second kind of air entrainment is due to breaking waves, coming from the interaction of several factors depending on the configuration: the incoming wave and a reflected one on the bow and/or the impact between the bow and the free surface. The breaking phenomena observed in configurations 2, 3 and 4 are similar. Only the magnitude and the frequency is changing with the configuration. The air entrainment by a breaking wave is more energetic and almost instantaneous. It can be seen on Fig. 12 that bubbles do not pass under the hull. As detailed in Section 3.1, the bubbles generated around the model are in the range of several millimetres and rise to the surface rapidly. These mechanisms observed in laboratory are similar to those encountered at sea, even if the quantity of air entrained and the size of bubbles are distinct.

The synchronism between the different cameras allows to correlate the free surface phenomenon and the generation of bubbles as can be seen in Figs. 13 and 14 for the breaking wave cloud case. On these figures are represented six instants of the air entrainment process acquired underwater (left images) and above the free surface by one of the two CMOS cameras (right images). The time interval between each moment is two images (0.13 s). The corresponding pitch, heave and free surface elevation at the center of gravity are represented on Fig. 15.

The three instants (t1, t2 an t3) of Fig. 13 correspond to a peak

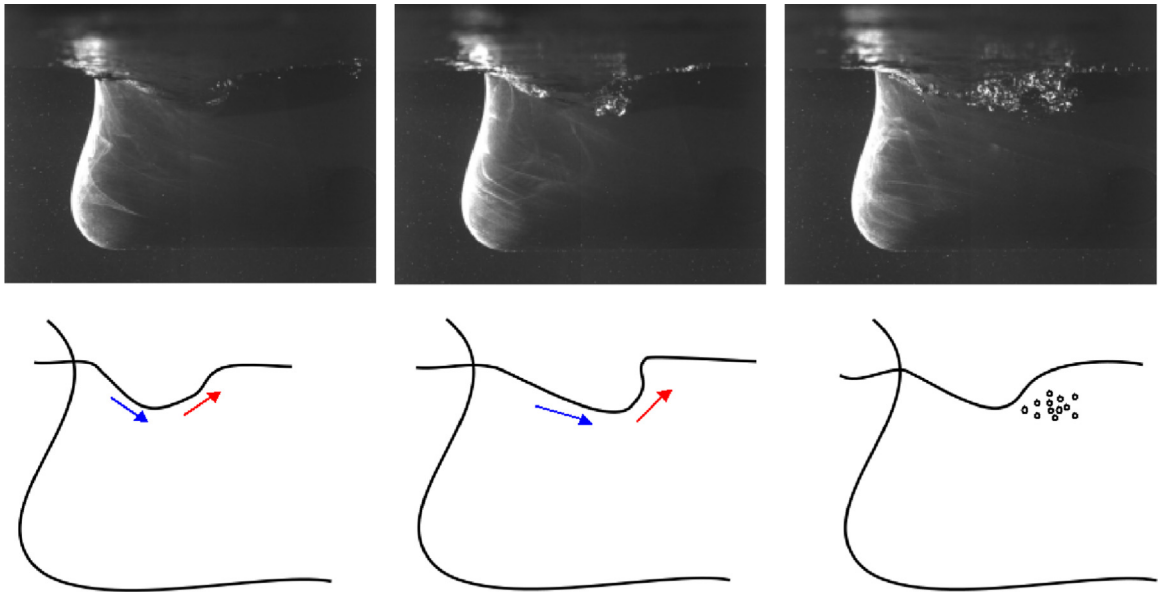

Fig. 11. Description of the vortex shedding clouds generation from the free surface distortion to the flow aeration, encountered in the fourth cases.

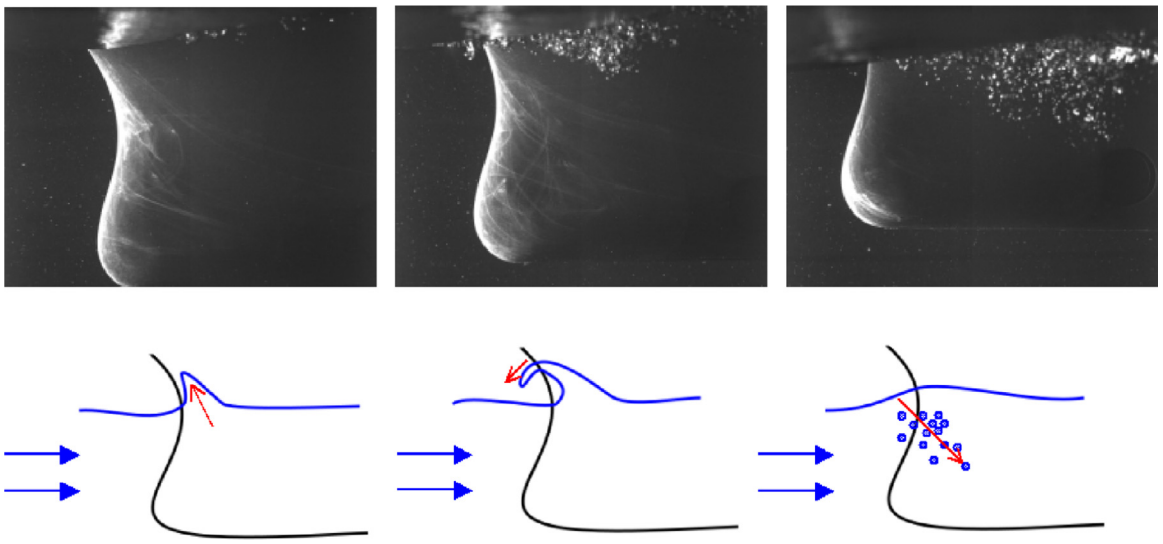

Fig. 12. Description of the breaking wave clouds generation from the generation of a reflective wave on the bow to the flow aeration, encountered only for cases 2–4.

of pitch. The front of the model impacts the free surface and the incoming wave, generating a breaking bow wave. The bubbles that can be seen on these pictures are due to a previous vortex shedding cloud. The bow wave is entirely formed at t3, and the impact occurs before t4.

In Fig. 14 (t4, t5 and t6) the bow is pulled up, and air is entrapped by the breaking wave. The bubble cloud formed is entrained down by the plunging jet velocity at the instant when the bow is highest.

The details of image analysis leading to bubble clouds surface and density, bubble depth penetration, cloud velocities, for both breaking wave and vortex shedding cases will be given in the second part of the paper.

4.2. *Bubble clouds frequency*

The frequency of each air entrainment mechanism for each configuration can be determined from video analysis of the underwater sequences directly by operators visualization (several operators have realized these analysis and obtain the same bubble clouds occurrence). The results obtained for the four cases are shown in Fig. 16. In the first case with current only, the bubble cloud frequency is low (<0.2 Hz) and only due to vortex shedding along the hull. This phenomenon is caused by the interaction between the bow shape and the highly turbulent incoming flow. In the second case with waves and current, breaking bow waves were observed. The proportion of bubble clouds generation increases to reach a cloud generation seven out of ten waves (0.59 Hz for clouds frequency compared to 0.85 Hz for the wave frequency). Here the two kinds of bubble clouds are encountered with approximately the same level of occurrence of vortex shedding cloud type as for the case 1. The breaking wave cloud type appears twice more frequently than the other one. For the case of hull motion under current (case 3), the bubble cloud occurrence is approximately twice than for case 1. Here also the two kinds of bubble clouds are encountered with similar level of occurrence for each of them. The hull motions generate less bubble clouds than waves (a cloud frequency of 0.40 Hz compared to 0.59 Hz). For the hull motion under waves and current (case 4), the combination of solicitations leads to an accumulation of effects until the

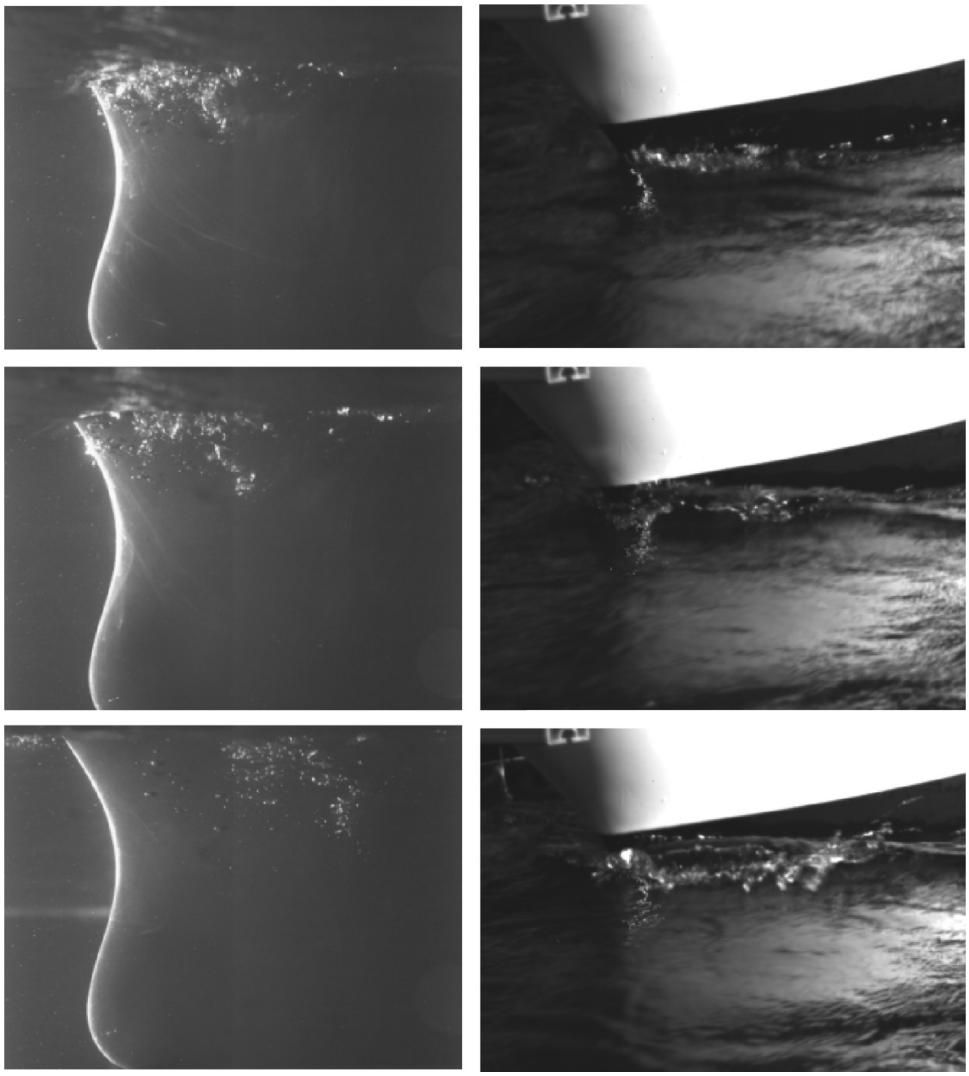

Fig. 13. Simultaneous visualizations of the generation of bubbles (left) and the breaking wave (right) during the breaking wave event (t1, t2 and t3).

generation of bubble cloud for nearly eight out of ten incoming wave (0.66 Hz). In this case, breaking wave cloud type is mainly encountered.

These frequency calculations were undertaken in 5 min sequences (250 wave periods). Air entrainment frequency were also calculated every 30 s in order to confirm the convergence of the results. Fig. 17 shows this process for the four configurations. In the second part of the paper, the influence of the tests parameters will be analysed (wave or motion amplitude and frequency for instance). For all these trials the recording sequences will be limited to 3 min (150 wave periods) and considered to be converged, thanks to the stability of the mean values obtained on longer periods as shown in Fig. 17.

5. Conclusion

The difficulty of observing bubble sweep-down on ship models during towing tank test led us to develop an original method to study this phenomenon. We demonstrate in this paper that a wave and current circulating tank is particularly well suited to achieve this goal. Even if scale effects discussed in Section 3.1 are significant, this methodology allows the quantification of the phenomena leading to bubble generation around the bow of a ship under waves and current. The observation window gives an easy and good view of the phenomenon. The use of the motion generator enables the study of wave and ship movement independently, while the specific turbulent current is a source of air entrainment. The methodology developed in this paper also allows to work on the bow model only, which was a significant progress for the study in such facility. In this configuration it was possible to observe simultaneously the free surface behaviour and the generation of bubbles. Two distinct mechanisms of air entrainment were encountered and described. The vortex shedding bubble clouds appear randomly in all the configurations tested, even without waves or motions. This phenomenon is due to the interaction between the turbulent flow and the specific bow shape of the *Pourquoi pas?*. On the other hand, the breaking wave clouds appear in the presence of relative motions between the free surface and the bow ship and more significantly under wave solicitations.

In the second part of the paper, image analysis will be used to analyse in detail these two kinds of bubble clouds formation. The impact of several parameters will be studied to understand the influence of each of them on the bubble generation. Therefore the influence of wave amplitude and frequency, motions amplitude

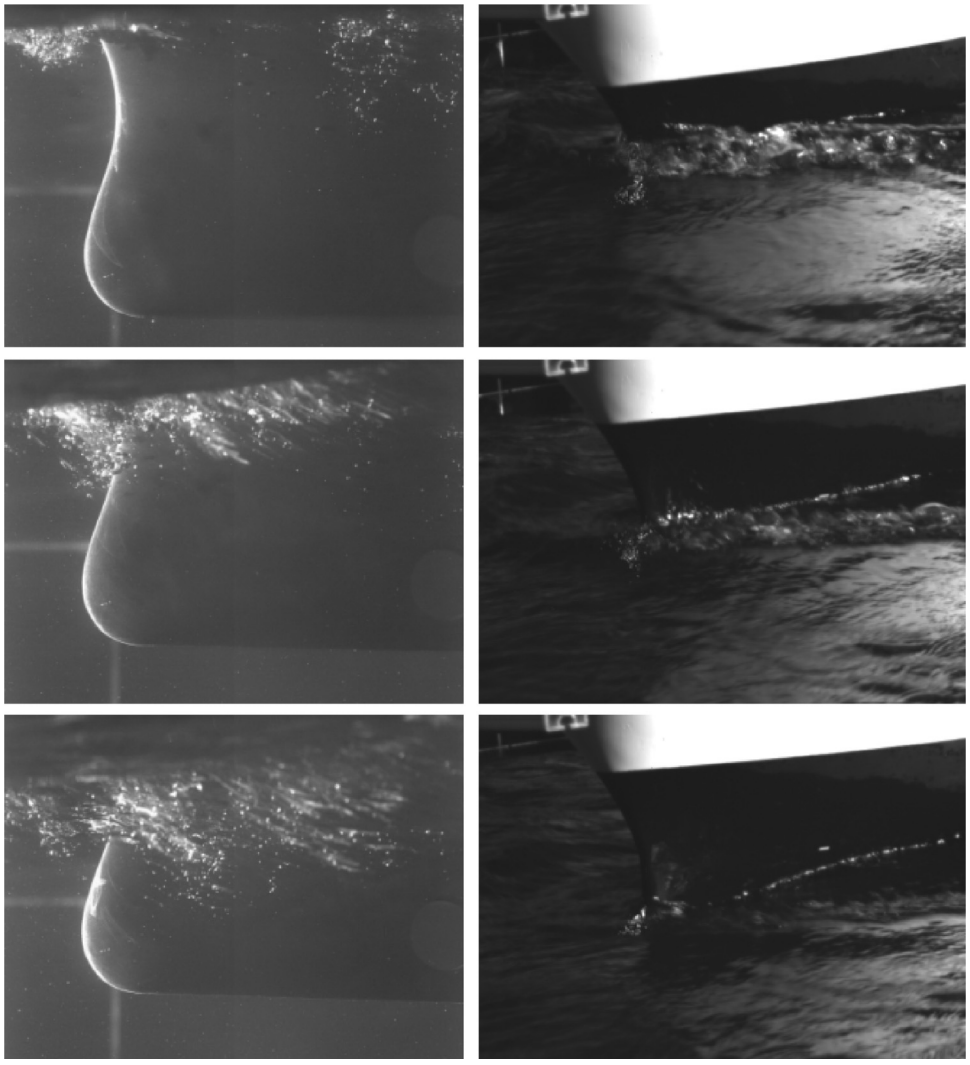

Fig. 14. Simultaneous visualizations of the generation of bubbles (left) and the breaking wave (right) during the breaking wave event (t4, t5 and t6).

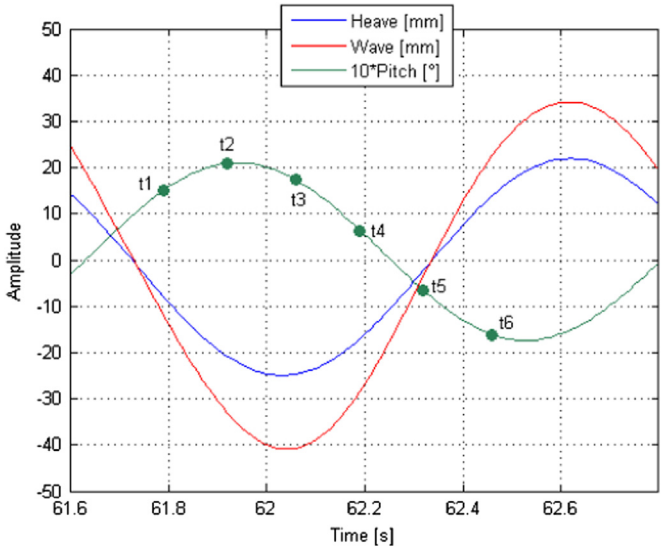

Fig. 15. Pitch, heave and free surface elevation (at the center of gravity) during instantaneous visualizations (t1 → t6) of breaking wave and air entrainment events.

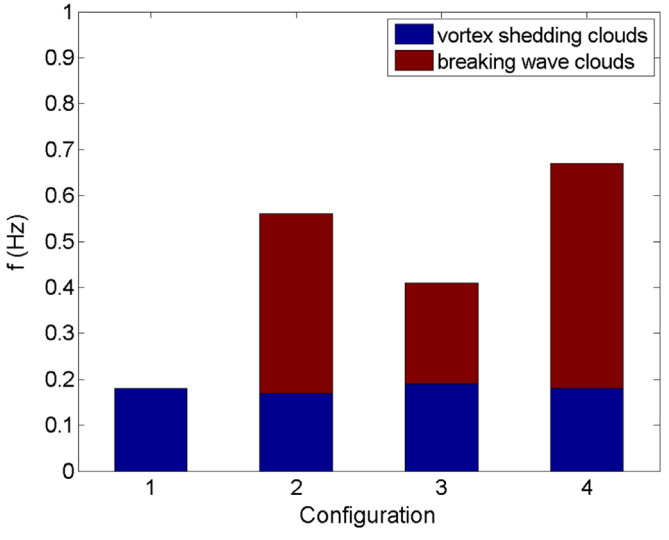

Fig. 16. Air entrainment frequency, breaking wave clouds and vortex shedding clouds, for the 4 test configurations.

and frequency, current speed, turbulence, phase shift between waves and motions will be studied.

Such results could be used for the validation of future numerical models searching to consider these phenomena. Moreover the instrumentation used in this method can also be involved in the acquisition of velocity maps of the flow around the

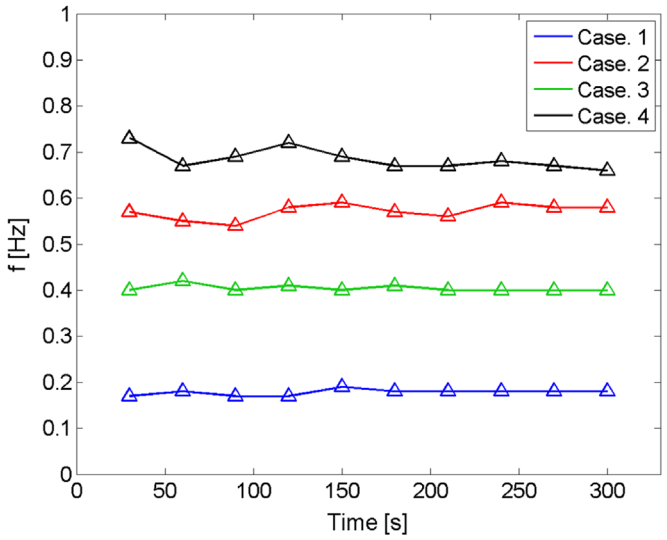

Fig. 17. Study of bubble clouds frequency convergence for the 4 test configurations.

bow, that are representative of real scale through the Froude similarity. By this way different bow shapes performances regarding the bubble sweep-down phenomena could be compared.

Acknowledgments

The authors gratefully acknowledge the DGA (the French Government Agency for Defense) and Ifremer for the financial support of co-financed PhD theses.

We also would like to thank Thomas Bacchetti and Jean-Valery Facq for their assistance in the design and set-up of these experiments.

References

Bouhoubeiny, E., Druault, P., Germain, G., 2014. Phase-average mean properties of turbulent flow developing around a fluttering sheet of net. Ocean Eng. 82, 160–168.

Carrica, P.M., Castro, A.M., Li, J., Politano, M., Hyman, M., 2012. Towards an air entrainment model. In: Proceedings of the 29th Symposium on Naval Hydrodynamics, Gotheburg, Sweden.

Castro, A.M., Li, J., Hyman, M., Carrica, P.M., 2014. Turbulent and cavity free surface bubble entrainment with application to ship hydrodynamics. In: Proceedings of the 30th Symposium on Naval Hydrodynamics, Hobart, Tasmania, Australia.

Cartmill, J.W., Su, M.Y., 1993. Bubble size distribution under saltwater and freshwater breaking waves. Dyn. Atmos. Oceans 20, 25–31.

Chanson, H., Cummings, P.D., 1994. Effects of plunging breakers on the gas contents in the oceans. Mar. Technol. Soc. J. 28, 22–32.

Cooper, E.B., 2012. The future RRS discovery. Ocean Challenge 19, 9–10.

Dalen, J., Løvik, A., 1981. The influence of wind-induced bubbles on echo integration surveys. J. Acoust. Soc. Am. 69, 1653–1659.

De Kat, J.O., Paulling, J.R., 2001. Prediction of extreme motions and capsizing of ships and offshore vehicles. In: Proceedings of the 20th OMAE Conference, Rio de Janeiro.

Delacroix, S., 2015. Caractérisation de la génération et de la propagation de bulles autour de la carène de navires scientifiques (Ph.D. thesis), Université de Bretagne Occidentale.

Delacroix, S., Germain, G., Berger, L., Billard, J.Y., 2016. Bubble sweep-down occurrence characterization on Research Vessels. Ocean Eng. 111, 34–42.

Delhommeau, G., Guilbaud, M., David, L., Yang, C., Noblesse, F., 2009. Boundary between unsteady and overturning ship bow wave regimes. J. Fluid Mech. 620, 167–175.

Deane, G.B., Stokes, M.D., 1999. Air entrainment processes and bubble size distributions in the surf zone. J. Phys. Oceanogr. 29, 1393–1403.

Deane, G.B., Stokes, M.D., 2002. Scale dependence of bubble creation mechanisms in breaking waves. Nature 418, 839–844.

Gaurier, B., Davies, P., Deuff, A., Germain, G., 2013. Flume tank characterization of marine current turbine blade behaviour under current and wave loading. Renew. Energy 59, 1–12.

Kracht, W., Finch, J.A., 2009. Bubble break-up and the role of frother and salt. Int. J. Miner. Process. 92, 153–161.

Ma, J., Oberai, A.A., Hyman, M.C., Drew, D.A., Lahey Jr, R.T., 2011. Two-fluid modeling of bubbly flows around surface ships using a phenomenological subgrid air entrainment model. Comput. Fluids 52, 50–57.

MARIN Technical report, Seakeeping Tests for the Research Vessel “Pourquoi pas?” Final report, Report No 18268-2-SMB.

Moraga, F.J., Carrica, P.M., Drew, D.A., Lahey Jr, R.T., 2008. Air entrainment model for breaking bow waves and naval surface ships. Comput. Fluids 37, 281–298.

New, A.L., 1992. Factors affecting the quality of shipboard acoustic Doppler current profiler data. Deep-Sea Res. 39, 1985–1996.

Noblesse, F., Delhommeau, G., Guilbaud, M., Hendrix, D., Yang, C., 2008. Simple analytical relations for ship bow waves. J. Fluid Mech. 600, 105–132.

Noblesse, F., Delhommeau, G., Guilbaud, M., Liu, H., Wan, D., Yang, C., 2013. Ship bow waves. J. Hydrodyn. 25, 491–501.

Rolland, D., Clark, P., 2010. Reducing bubble sweepdown effects on research vessels. OCEANS'10. IEEE, Sydney.

Shabangu, F.W., Ona, E., Yemane, D., 2014. Measurements of acoustic attenuation at 38 kHz by wind-induced air bubbles with suggested correction factors for hull-mounted transducers. Fish. Res. 151, 47–56.

Shakeri, M., Tavakolinejad, M., Duncan, J.H., 2009. An experimental investigation of divergent bow waves simulated by a two-dimensional plus temporal wave marker technique. J. Fluid Mech. 634, 217–243.

Tavakolinejad, M., 2010. Air bubble entrainment by breaking bow waves simulated by a 2D+T technique (Ph.D. thesis), University of Maryland.

Trevorrow, M.V., 2003. Measurements of near-surface bubble plumes in the open ocean with implications for high-frequency sonar performance. J. Acoust. Soc. Am. 114.

Von Bröckel, K., 2014. Echo Sounders versus Air Bubbles in Research Vessels. Hydro Int., January/February, 14–17.

Waniewski, T.A., Brennen, C.E., Raichlen, F., Measurements of air entrainment by bow waves. J. Fluids Eng. 123, 57–63.